Detection of refractive index and imperfection in thin film transparent polymer by back focal plane imaging.

Hodaya Kilmovsky[1,2], Omer Shavit[1,2,3], *Martin* Oheim[3], and *Adi* Salomon*[1,2,3]

[1] Chemistry department, Bar-Ilan University, 529000, Ramat-Gan, Israel
[2] Institute of Nanotechnology and Advanced Materials (BINA), Bar-Ilan University, 529000, Ramat-Gan, Israel
[3] Université Paris Cité, SPPIN Saints-Pères Paris Institute for the Neurosciences, CNRS, Paris, France

Abstract. Emission patterns from molecules at interfaces encode many details about their local environment and their axial position, along the microscope's optical axis. We introduce an advanced approach that synergizes back focal plane (BFP) imaging with innovative 'smart' surfaces make surface imaging more qualitative, more reliable, and more robust. Our method is particularly focused on accurately measuring the refractive index (RI) of transparent thin films and their imperfections close to the interfaces. Our technique utilizes a 'smart' surface, which features a uniform fluorescent thin film of about 4 nm thickness together with back-focal plane (BFP) imaging. We manage to detect bubbles or other imperfection in 100 nm thin film of polymer with RI of 1.34.

1 INTRODUCTION

The challenge of obtaining precise, quantitative, nano-scale measurements along z, i.e., the microscope's optical axis has been a significant hurdle in traditional and super-resolution optical microscopies. Electron microscopes, on the other hand, falls short in selectively exploring in-operando interface/surface activities.

Despite significant advancements in nanoscience and nanotechnology over the past three decades, a comprehensive understanding and quantification of near-surface phenomena—ranging from biofilm growth and crystallization to cellular signaling or various chemical processes like surface catalysis, electrode ageing and others —still present substantial challenges.

By using BFP imaging combined with total internal reflection fluorescence (TIRF) microscopy, we measured the refractive index of a transparent thin film deposited onto our 'smart surface' and we even sensed imperfections in the film, such as bubbles or other faults, close to the interface.

Our smart surface is composed of a 5-nm homogenous layer of fluorophores (H_6TPPS) in its J-aggregate form.[1] This emitter layer is deposited onto a thin, transparent polymer film having a RI of 1.33 (My133-MC). The result is a flat, homogeneous emitter layer at a controlled axial distance from the surface[2], typically about 100 nm, and which can be covered with the same polymer, or other substances to be characterized.

1.1 Emitter at the interface

The emission pattern of a fluorophore changes when it is positioned near an interface compared to when it is in a homogenous medium. Close to the interface, the evanescent component of a molecular dipole's near-field emission can couple to the interface, transitioning into a propagative mode. This is akin to the excitation evanescent field in TIRF microscopy, which necessitates supercritical illumination angles for observation. Consequently, this type of emission must also propagate at supercritical angles, which are typically not accessible for conventional far-field dipole emissions. As a result, fluorophores near an interface tend to emit more into the medium with the higher refractive index (n_2), predominantly at angles beyond the critical emission angle $\vartheta_c = asin(n_1/n_2)$, Fig.1. By analyzing supercritical angle fluorescence (SAF) in pupil plane (BFP) images, we determine ϑ_c, and thereby calculate the refractive index (RI) of the fluorophores' local environment, n_1, using $n_1 = f/r_c$, where r_c represents the equivalent critical radius, and f denotes the focal length of the objective.[2-5]

In the current communication, we use this technique to detect defects of in the My-133-MC polymer film deposited onto our smart surface.

* Corresponding author: adi.salomon@biu.ac.il

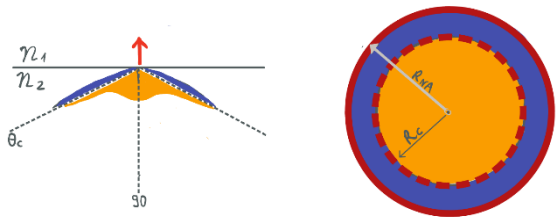

Fig. 1. *Distance-dependent modification of the fluorophore radiation pattern. Left* , emission pattern of a dipole at the interface of two media having different RI, n_1 in which the dipole is located, and n_2, of the substrate. For axial distances below $\lambda/2$, the near-field emission component of the near-interface dipole can couple to the interface and become propagative, which is seen in the denser medium as light travelling above the emission critical angle $\vartheta > \vartheta c$. *Right*, corresponding BFP image with the measures mentioned in the main text. Color code as on the left. NA - numerical aperture

To obtain a uniform and homogenous My-133-MC polymer films, we filtered the solution to remove air bubbles. Yet, BFP images sometimes unexpectedly revealed a double-ring structure, featuring two intensity transitions, one at RI = 1.33 and another one at RI = 1, **Fig. 2a**. The inner ring was typically dimmer compared to the outer one, see *red arrow* on panel (a), and the diameter of the outer ring corresponded to that observed for the majority of produced polymer samples (*right*).

We reasoned that such double-ring pattern could result if some - but not all - of the fluorophores were exposed to air rather than polymer. Such a non-homogeneous dye environment could result from cavities, cracks or air-bubbles in the polymer (see **Fig. 3**). A *post-hoc* FIB cross-section on these samples confirmed the presence of µm-sized bubbles in the polymer layer, **Fig. 2b**. We note, however, that the bubble size is probably an overestimate of their true diameter, given that SEM images were taken in vacuum. Dual RIs could also appear when cracks or dimples are present. Fig. 2c illustrates such an example where a marked RI rise was observed upon wetting the polymer surface. Starting from an air-dominated situation, pipetting a drop of polymer onto the surface changed the RI changes – from 1 (green), to 1.3 (blue) with an abrupt change occurring at the moment of the deposit of the drop (red), i.e. two interfaces.

We conclude that the information contained in the fluorophore radiation pattern does not only permit precise thin-layer refractometry[2-5] but it also reveals imperfections, the detection of which requires otherwise more involved, lengthy and expensive experiments under vacuum. The time-series in **Fig.2c** furthermore shows that our technique permits time-resolved measurements and *in operando* refractometry, which is an important feature for sensors and thin-film devices. Based on this SAF-based BFP-image refractometry, we retained only samples that passed the quality gate of a single-ring BFP pattern.

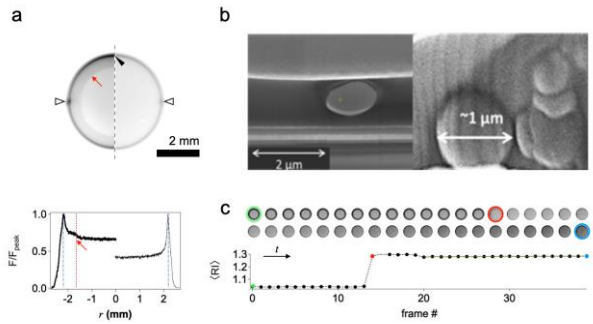

Fig. 2 *BFP-based detection of flaws in nano-fabrication*. (a), *left* half, example BFP image of an imperfect polymer layer displaying a double-ring structure at RIs corresponding to both air (red arrow) and My-133-MC (black arrowhead). *Right*, single-ring structure observed for a flawless sample for comparison. Intensity of the left half image increased for better visibility, contrast is inverted, as in fig.2. *Bottom*, corresponding normalized-intensity line profiles. Note the little kink on the left profile (*red* arrow), absent from the right. Dash-dotted and dotted lines indicate RI 1.33 and 1, respectively. (b), two examples of *post-hoc* FIB cross-sections of imperfect polymer films. (c), example of a My-133-MC polymer layer with cracks. *Top*, time-lapse BFP-image series and SAF-derived RI, *bottom*. At frame #14, a drop of polymer was pipetted on top of the sample, increasing the measured RI from close to 1 to 1.33. Colored rings and spots, respectively, identify corresponding time frames.

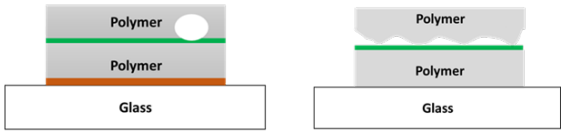

Fig. 3. *Possible explanations for a double-ring emission pattern.* Schematic illustrations show air bubbles in the spacer layer (*left*) or an imperfect coverage of the TPPS-dye layer (*right*) as possible reasons. Drawings are not to scale.

References

1. A. Weissman, H. Klimovsky, D. Harel, R. Ron, M. Oheim A. Salomon Langmuir, 36 (2020), p. 844
2. H. Klimovsky, O. Shavit, C. Julien, I. Olvesko, M. Hamode, Y. Abulafia, H. Suaudeau, V. Armand, M. Oheim and A. Salomon. Adv. Opt. Mat. **11**, 2203080, (2023)
3. M. Brunstein, L. Roy, M. Oheim, *Biophys. J.* 2017, **112**, 1940.
4. B. Ferdman, L. E. Weiss, O. Alalouf, Y. Haimovich, Y. Shechtman, *ACS Nano* 2018, **12**, 11892.
5. M. Oheim, A. Salomon, M. Brunstein, *Biochem. Biophys. Perspect. Mar. Biol.* 2020, **118**, 2339.